Atmos. Chem. Phys. Discuss., 11, 8431–8460, 2011
www.atmos-chem-phys-discuss.net/11/8431/2011/
doi:10.5194/acpd-11-8431-2011

Atmospheric Chemistry and Physics Discussions

Coupled vs. decoupled boundary layers in VOCALS-REx

C. R. Jones[1], **C. S. Bretherton**[2], **and D. Leon**[3]

[1]Department of Applied Mathematics, University of Washington, Seattle, Washington, USA
[2]Department of Atmospheric Sciences, University of Washington, Seattle, Washington, USA
[3]Department of Atmospheric Science, University of Wyoming, Laramie, Wyoming, USA

Received: 3 March 2011 – Accepted: 8 March 2011 – Published: 11 March 2011

Correspondence to: C. R. Jones (cjones@amath.washington.edu)

Published by Copernicus Publications on behalf of the European Geosciences Union.

Abstract

We analyze the extent of subtropical stratocumulus-capped boundary layer decoupling and its relation to other boundary-layer characteristics and forcings using aircraft observations from VOCALS-REx along a swath of the subtropical southeast Pacific Ocean running west 1600 km from the coast of Northern Chile. We develop two complementary and consistent measures of decoupling. The first is based on boundary layer moisture stratification in flight profiles from near the surface to above the capping inversion, and the second is based the difference between the lifted condensation level (LCL) and a mean lidar-derived cloud base measured on flight legs at 150 m altitude. Most flights took place during early-mid morning, well before the peak in insolation-induced decoupling.

We find that the boundary layer is typically shallower, drier, and well mixed near the shore, and tends to deepen, decouple, and produce more drizzle further offshore to the west. Decoupling is strongly correlated to the "well-mixed cloud thickness", defined as the difference between the capping inversion height and the LCL; other factors such as wind speed, cloud droplet concentration, and inversion thermodynamic jumps have little additional explanatory power. The results are broadly consistent with the deepening-warming theory of decoupling.

In the deeper boundary layers observed well offshore, there was frequently nearly 100% boundary-layer cloud cover despite pronounced decoupling. The cloud cover was more strongly correlated to a κ parameter related to the inversion jumps of humidity and temperature, though the exact functional relation is slightly different than found in prior large-eddy simulation studies.

ACPD
11, 8431–8460, 2011

1 Introduction

The simplest realistic model of subtropical stratocumulus consists of a single, well-mixed boundary layer in which vigorous turbulence stirs the moist-conserved variables liquid potential temperature θ_ℓ and total water mixing ratio

$$q_T = q_\ell + q_v \quad (1)$$

into vertically uniform profiles below a capping temperature inversion at height z_i. Here, q_ℓ is the liquid water content and q_v is the water vapor mixing ratio. Mixed-layer models (MLMs) (e. g. Lilly, 1968), which prognose the evolution of the boundary-layer θ_ℓ, q_T and z_i assuming this well-mixed structure, have provided many insights into the structure and maintenance of subtropical stratocumulus layers.

In contrast, decoupling of the boundary layer occurs when the turbulence does not maintain a well-mixed layer. The radiatively driven turbulence in the cloud layer becomes separated from that of the surface-flux driven subcloud layer, and the two layers become "decoupled" in the sense that each layer itself is well-mixed, but mixing between the cloud and subcloud layer is inhibited by the presence of a stable layer between them (Nicholls, 1984). In this study, we loosely define a decoupled boundary layer as any layer that is not well-mixed, and often refer to a well-mixed layer as being coupled. Nicholls (1984) used a diagnostic MLM to demonstrate that correctly accounting for decoupling is necessary for a model to adequately reproduce the observed diurnal cycle of stratocumulus.

Decoupling is driven by a number of factors that promote internal stratification of the boundary layer (Bretherton and Wyant, 1997). Daytime insolation drives diurnal decoupling by heating the cloud layer much more than the underlying subcloud layer (e.g. Nicholls, 1984; Turton and Nicholls, 1987). The measurements considered in the current study occur primarily in the morning, so direct diurnal forcing is not the dominant mechanism we observe. Precipitation, even when it mainly evaporates before reaching the surface, promotes "drizzle decoupling" by heating the cloud layer and cooling

ACPD
11, 8431–8460, 2011

the subcloud layer. It can be important even in thin cloud layers when cloud condensation nucleii are sparse. Deepening-warming decoupling, introduced by Bretherton and Wyant (1997), can occur as a well-mixed stratocumulus-capped boundary layer deepens by advecting over warmer sea surface temperature (SST). As the layer deepens, increasing latent heat fluxes increase buoyancy production of turbulence in the cloud layer and (through entrainment feedback) drive buoyancy fluxes negative in the subcloud layer until decoupling results.

Our goal in this manuscript is to classify the extent of decoupling observed during the VOCALS Regional Experiment (VOCALS-REx) in October–November 2008, which sampled the Southeast Pacific marine boundary layer off the coast of Chile. This region is home to a large and persistent subtropical stratocumulus deck. As summarized by Bretherton et al. (2010), near the coast the boundary layer is typified by a strong (10–12 K) capping inversion with a typical depth of approximately 1000 m and a typical cloud droplet number concentration of 250 cm^{-3}, while 1500 km to the west the typical depth is 1600 m and the typical cloud droplet concentration is less than 100 cm^{-3}. The boundary layer tends to be well-mixed and non-drizzling near the shore, with a greater tendency to decouple and drizzle further offshore.

This study is based on measurements from 13 research flights (RFs) of one of the two VOCALS long-range aircraft, the NSF C-130. The C-130 sampled from 70°–85° W between 17° and 30° S, with most measurements occurring from pre-dawn to mid-afternoon. A typical RF consisted of a repeated sequence of level legs, including a subcloud leg (150 m above sea level), an in-cloud leg (slightly under the capping inversion), and an above-cloud leg (100–300 m above the inversion), with regular deep profiles extending from 150 m up to 3000 m. See Wood et al. (2011) for a more complete description of VOCALS-REx.

Figure 1 shows a time-height section of reflectivity from the vertically-pointing beams of the University of Wyoming Cloud Radar (WCR) for RF04, a typical flight surveying the boundary layer structure along 20° S. This illustrates the VOCALS flight plan as well as commonly-observed features of the boundary layer structure in the region. It can be compared with a similar figure for RF03 in Bretherton et al. (2010). The C-130 flight path is shown in grey; a radar dead zone is visible around the flight path. The flight starts near the shore, where the nocturnal boundary layer is well-mixed, nondrizzling, and shallow, with an inversion around 1200 m. As the flight proceeds to the west, the inversion height rises, drizzle increases, organized in mesoscale cells, and the boundary layer becomes decoupled, as indicated by the divergence of the LCL based on in-situ measurements, shown in green, and the University of Wyoming Cloud Lidar (WCL) cloud base measured from an upward pointing lidar during subcloud legs flown at approximately 150 m above sea level (black). During the return flight from 85° W to the coast the boundary layer again becomes shallower and coupled near the coast, even though it is now nearly noon local time.

The many C-130 flights during VOCALS-REx provide a rich database with which to study decoupling across a range of boundary layer types. In-situ thermodynamic profiles and radar/lidar measurements from subcloud legs provide complementary views of decoupling. Our goal is to use this dataset to statistically characterize decoupling and its relation to cloud cover and thickness, precipitation, and inversion jumps during VOCALS-REx.

2 Decoupling measures and data sources

2.1 Data sources

This analysis utilizes measurements made by the NSF C-130 aircraft and recorded at 1 Hz. In addition to in-situ atmospheric state measurements, we also utilize the WCR to deduce the cloud top and column-maximum radar reflectivity (a precipitation proxy). WCL-derived measurements of cloud base are used during subcloud legs.

The NSF C-130 measurement data are publicly available on the VOCALS Project web page managed by NCAR/EOL[1]. WCR and WCL data used in this study will also

[1] http://www.eol.ucar.edu/projects/vocals/dm/index.html

ACPD
11, 8431–8460, 2011

soon become publicly archived available at this site. Wood et al. (2011) discusses data availability and access in further detail, along with a summary of the various measurements taken by each of the aircraft that took part in VOCALS-REx.

For ease of comparison, the profile data were averaged within 10 meter vertical bins. Corrections to the humidity, measured using the NSF C-130 Lyman-alpha hygrometer, have been applied following Bretherton et al. (2010). These corrections primarily impact the derived LCL, and increase the measured vapor mixing ratio by approximately 5%.

2.2 Profile-based decoupling measure Δq

We use two complementary methods for identifying a decoupled versus well-mixed boundary layer, one of which applies to the profiles while the other utilizes the subcloud legs.

The profile-based method compares the total moisture mixing ratio near the surface to that just below the inversion, and provides a direct, local means of interpreting the vertical structure of the boundary layer with regards to decoupling.

Figire 2 shows a typical well-mixed (left) and decoupled (right) profile from VOCALS-REx. In the well-mixed case, the total water mixing ratio q_T and liquid potential temperature θ_ℓ remain relatively constant with height below the inversion. In the decoupled case, there appear to be two well-mixed layers, separated by a 100 m deep stable layer centered at an altitude of 700 m.

Our profile measure of decoupling seeks to capture this behavior by defining a decoupling index

$$\Delta q = q_{\text{bot}} - q_{\text{top}}, \tag{2}$$

where q_{bot} is the mean q_T in the bottom 25% of the boundary layer below the inversion, and q_{top} is the mean total mixing ratio in the top 25% of the boundary layer below the inversion. For each profile the height of the inversion, z_i, is determined as the height at

ACPD

11, 8431–8460, 2011

VOCALS decoupling

C. R. Jones et al.

which the temperature is a minimum provided the relative humidity is at least 45%. We use 110 C-130 profiles during VOCALS-REx that extend from below $0.25z_i$ through the inversion, and that lie north of 25° S. Two coastal aerosol flights went south of 25° S, where they sampled a shallow boundary layer under strong synoptically-driven subsidence with a diffuse inversion and patchy cloud cover atypical of the rest of the VOCALS region considered in this study.

We identify profiles with $|\Delta q| < 0.5\,\mathrm{g\,kg^{-1}}$ as well-mixed, and those with $|\Delta q| > 0.5\,\mathrm{g\,kg^{-1}}$ as decoupled. This threshold is somewhat arbitrary, but seems to differentiate between those profiles which have a distinct humidity decrease just above the LCL (Fig. 2b), which we regard as diagnostic of decoupling, from those that do not.

Figure 3 shows a histogram of the profile decoupling metric for the REx profiles included in this analysis. The well-mixed threshold is indicated on the plot by the red vertical lines. Approximately 36% of profiles in VOCALS-REx were classified as well-mixed.

2.3 Subcloud decoupling measure Δz_b

Another "subcloud" measure of decoupling is provided by the C-130 subcloud legs flown at approximately 150 m above sea level, based on comparison of the the aircraft-measured LCL and the WCL-measured cloud base z_b on these legs. When the boundary layer is well-mixed, the LCL and cloud base measurements are in close agreement, but in the decoupled regime the LCL and cloud base may diverge by as much as several hundred meters.

FIgure 4 shows the LCL and cloud base measurements for the subcloud legs adjacent to the profiles in Fig. 2. In the well-mixed case (left) the LCL and cloud base are close; their difference fluctuates around 50 m (this value is sensitive to humidity calibrations applied to the data and should be regarded as having a roughly 50 m uncertainty; see Bretherton et al., 2010). Their "mesoscale" variability also correlates well (here mesoscale refers to scales much longer than 10 s of flight time, which at the $100\,\mathrm{m\,s^{-1}}$ nominal aircraft speed corresponds to distances much longer than 1 km). By

ACPD
11, 8431–8460, 2011

contrast, the decoupled case (right) shows tremendous variability in both the LCL and WCL cloud base. The difference between the cloud base and the LCL ranges between 100 and 1000 m across the 700 s (70 km) leg.

A subcloud decoupling index was computed for each subcloud leg as the leg-mean difference between the z_b and the LCL:

$$\Delta z_b = \overline{z_b - z_{\mathrm{LCL}}}. \tag{3}$$

2.4 Relation between Δz_b and Δq

A Δz_b threshold for decoupling that is consistent with the profile-based Δq threshold can be derived from a thermodynamic argument. The LCL is based on the aircraft measured temperature, pressure, and moisture during a subcloud leg flown at an altitude of $z_{\mathrm{SC}} \approx 150$ m. Thus, the saturation mixing ratio $q^*(p_{\mathrm{LCL}}, T_{\mathrm{LCL}}) = q_v(z_{\mathrm{SC}})$, where p_{LCL} and T_{LCL} are the temperature and pressure derived by dry-adiabatically lifting mean subcloud-layer air to the height z_{LCL}. On the other hand, the cloud base z_b is the exact level at which the air becomes saturated, so $q(z_b) = q^*(p_b, T(z_b))$.

To compare the two metrics, we neglect the weak dependence of q^* on pressure, by approximating the true pressure with a reference pressure p_0 close to the true cloud base and LCL pressures. We assume that the cloud base humidity is approximately equal to the mean q_T over the top 25% of the boundary layer, and that $q_v(z_{\mathrm{SC}})$ is approximately equal to the humidity averaged over the bottom 25% of the boundary layer below the inversion. Then

$$\begin{aligned}\Delta q &\approx q_v(z_{\mathrm{SC}}) - q_v(z_b)\\ &= q^*(p_{\mathrm{LCL}}, T_{\mathrm{LCL}}) - q^*(p_b, T_{\mathrm{da}}(z_b))\\ &\quad - [q^*(p_b, T(z_b)) - q^*(p_b, T_{\mathrm{da}}(z_b))]\\ &\approx -\left(\frac{dq^*}{dz}\right)_{\mathrm{da}}(z_b - z_{\mathrm{LCL}}) - \frac{s(z_b) - s(z_{\mathrm{SC}})}{c_p}\frac{\partial q^*}{\partial T}.\end{aligned} \tag{4}$$

ACPD
11, 8431–8460, 2011

Here the subscript "da" indicates a dry-adiabatic and hydrostatic vertical displacement, and $s = c_p T + gz$ denotes the dry static energy.

If we assume that the actual temperature change between 150 m and the cloud base approximately follows a dry adiabat along which s is constant, we can neglect the second term on the right hand side. Then

$$\Delta q \approx -\left(\frac{dq^*}{dz}\right)_{\text{da}} (z_b - z_{\text{LCL}}). \tag{5}$$

At a characteristic boundary layer pressure of 950 hPa and temperature of 285 K $(dq^*/dz)_{\text{da}} = 0.0048\,\text{g kg}^{-1}\text{m}^{-1}$. Then (5) implies that $\Delta q = 0.5\,\text{g kg}^{-1}$ corresponds to $\Delta z_b \approx 100\,\text{m}$.

Because the actual temperature lapse rate is less than dry-adiabatic, the second term on the right hand side of the more accurate expression (4) is negative, and the needed Δz_b is larger. After considering this correction, we find that for our profiles, a threshold of $\Delta q = 0.5\,\text{g kg}^{-1}$ is typically equivalent to a $\Delta z_b \approx 125\,\text{m}$. Hence, a subcloud leg is considered well-mixed if $\Delta z_b < 125\,\text{m}$ and decoupled otherwise.

Figure 5 shows the consistency of the Δq and Δz_b measures. In this figure, Δq for each profile with an adjacent (occuring within 5 min) subcloud leg are matched with the corresponding Δz_b. The dashed black line indicates the linear relationship $\Delta z_b/\Delta q = 125\,\text{m}/(0.5\,\text{g kg}^{-1})$ obtained from the thermodynamic argument. The dashed red line is the linear least squares fit. As expected, there is a strong correlation between Δq and Δz_b; some scatter is expected because Δq comes from a single profile while Δz_b is an average over a leg that is near to the profile but does not overlap it, and because there is some variability in the temperature lapse rate beneath the cloud base.

2.5 Decoupling vs. drizzle from the subcloud legs

The subcloud legs are long enough to meaningfully characterize the average cloud-base precipitation. Since the precipitation of drizzle-size and larger droplets in drizzling

Discussion Paper | Discussion Paper | Discussion Paper | Discussion Paper |

ACPD
11, 8431–8460, 2011

VOCALS decoupling

C. R. Jones et al.

Title Page
Abstract Introduction
Conclusions References
Tables Figures
◀| |▶
◀ ▶
Back Close
Full Screen / Esc

Printer-friendly Version
Interactive Discussion

stratocumulus typically maximizes near the cloud base, we use as a drizzle proxy the leg-mean of the maximum cloud radar reflectivity Z_{max} in the boundary-layer column above the aircraft (sampled at 1 Hz), converted to a decibel scale:

$$dBZ = 10\log_{10}(\overline{Z_{\text{max}}}). \tag{6}$$

We define $dBZ > 0$ as heavy drizzle, $-10 < dBZ < 0$ as light drizzle, and $dBZ < -10$ as no (i.e. negligible) drizzle.

Figure 6 shows a histogram of the subcloud decoupling metric for all C-130 subcloud legs during VOCALS-REx, categorized by drizzle intensity. Approximately 40% of subcloud legs are found to have $\Delta z_b < 125$ m, in reasonable agreement with the fraction of well-mixed profiles. There is some correlation between decoupling and drizzle; in particular all heavily drizzling regions are classified as decoupled.

3 Correlation of decoupling with boundary-layer characteristics

The best correlate we found for decoupling in the REx dataset is the "mixed layer cloud thickness" $\Delta z_M = \overline{z_i - z_{\text{LCL}}}$, the thickness the cloud layer *would* have if the boundary layer was well-mixed and had the thermodynamic characteristics of the subcloud layer. One might expect that the mixed layer cloud thickness would correlate with decoupling based on arguments of Bretherton and Wyant (1997). Consider two cloud-topped mixed layers with identical z_i and θ_ℓ, one of which is slightly moister than the other so as to support a thicker cloud layer. The thicker cloud layer generates more entrainment to drive downward subcloud buoyancy fluxes that will decouple the boundary layer. The reason the thicker cloud generates more entrainment is that entrainment is driven by in-cloud turbulence, whose primary source is turbulent buoyancy fluxes. The turbulent buoyancy fluxes are large within the cloud layer and small or negative below the cloud. Hence, a thicker cloud layer will produce more turbulence and entrainment, which favors decoupling.

ACPD
11, 8431–8460, 2011

Figure 7 shows the longitudinal variation of decoupling and drizzle for the subcloud legs plotted versus Δz_M. The mixed layer cloud depth tends to increase from east to west. When Δz_M is shallow, the boundary layer typically remains well-mixed with little to no drizzle. As Δz_M increases above 500 m, the boundary layer tends to decouple and drizzle. Interpreted in this manner, the decoupling of the boundary layer further to the west is associated with larger Δz_M, which in turn reflects the westward increase in inversion height with no corresponding systematic increase in LCL. The relation between mixed layer cloud thickness, drizzle, and decoupling has little longitudinal dependence, even though there is a systematic decrease in boundary-layer accumulation-mode aerosol and cloud droplet concentrations to the west.

Several VOCALS-REx flights were devoted to investigating pockets of open convection (POCs). Even profiles within POCs, shown in Fig. 7 as open symbols, which have particularly low droplet concentrations, do not greatly deviate from the longitude-mean trends, although as expected they do seem to have somewhat higher drizzle intensities for a given well-mixed cloud thickness. These results suggest that while aerosol-cloud interactions may modulate decoupling in the VOCALS region, they are not its dominant controlling factor.

Figure 8 shows the longitudinal variation of decoupling using the profiles instead of the subcloud legs. The LCL was determined as an average value calculated between 150 m–200 m altitude during the profile. The general features are similar to those shown in Fig. 7 for the subcloud leg, but the separation between the well-mixed and decoupled legs is not nearly as sharp. This is to be expected, since the subcloud measurements are based on leg means (and as such capture the averaged properties over approximately 60 km), whereas the profiles are based on a single ascent or descent, which is more susceptible to local fluctuations.

The profiles are not categorized by drizzle intensity since the uncertainty in measuring the maximum radar reflectivity from the cloud base due to the radar direction and radar dead zone during profiles renders the measurements significantly less meaningful than the corresponding subcloud measurement of dBZ.

ACPD
11, 8431–8460, 2011

The VOCALS-REx research flights occurred mainly during the morning, and span too limited a range of times of day to usefully study the diurnal variation of decoupling in the VOCALS region; in fact we had difficulty detecting a diurnal signature of decoupling at any latitude using our two measures and datasets.

However, our findings are consistent with the deepening-warming mechanism for decoupling described in Bretherton and Wyant (1997). Using a mixed layer model, the authors identify the surface latent heat flux (LHF), net radiative flux divergence across the boundary layer ΔF_R, and z_b/z_i as important quantities controlling the onset of decoupling. In particular, for the highly idealized case of a steady-state, non-precipitating, well-mixed stratocumulus-capped boundary layer, they obtained the following condition for the development of a layer of negative subcloud buoyancy flux (necessary for decoupling to occur):

$$\frac{\Delta F_R}{\mathrm{LHF}} < A\eta \frac{\Delta z_M}{z_i}, \tag{7}$$

where A is the entrainment efficiency, and $\eta \approx 0.9$ is a thermodynamic variable. Based on an analysis of earlier ship-based observations in the VOCALS region, Caldwell et al. (2005) inferred $A \approx 1.1$. Precipitation, horizontal advection and other characteristics of the boundary layer can be accounted as correction terms to ΔF_R in Eq. (7) (Bretherton and Wyant, 1997), but these correction terms are difficult to reliably estimate from the available data, so here we will just use Eq. (7) as a framework for interpreting the role of different environmental factors in the decoupling observed in VOCALS-REx.

For the inferred $A = 1.1$, the right-hand side of Eq. (7) is approximately equal to $\Delta z_M/z_i$. That is, the decoupling criterion is more likely to be satisfied if $\Delta z_M/z_i$ is larger, consistent with the results of $\Delta z_M/z_i$ ranges shown in Fig. 7. A typical value of $\Delta z_M/z_i$ ranges from 0.3 for subcloud legs near the coast to 0.6 for legs at 85° W.

We also have attempted to evaluate the left hand side of Eq. (7). The overall result is that in the VOCALS dataset, it is significant but less important in regulating decoupling than is $\Delta z_M/z_i$, and tends to act in the same sense of promoting more decoupling further to the west.

ACPD
11, 8431–8460, 2011

The LHF was estimated using a bulk aerodynamic relationship

$$\mathrm{LHF} = \rho_{\mathrm{ref}} L C_T V (q_{ts} - q_{tM}), \tag{8}$$

where $C_T \approx 0.001$ is a transfer coefficient, V is the mean horizontal wind speed during a 150 m subcloud leg, q_{ts} is the water saturation mixing ratio at SST (multiplied by 0.981 to account for ocean salinity), q_{tM} is mixed layer mixing ratio, taken to be the leg-mean q_T, L is the latent heat of vaporization for water, and ρ_{ref} is a reference air density. When binned into 5° longitude ranges 70°–75° (near shore), 75°–80°, and 80°–86° W (far west), the mean LHF increases from 72 W m^{-2} near shore to 126 W m^{-2} in the far west, an increase of 75%. The increase of LHF to the west tends to further promote decoupling, since an increase in LHF leads to an increase in the cloud base buoyancy flux jump (Bretherton and Wyant, 1997).

The radiative flux divergence across the boundary layer, measured on a leg-by-leg basis following the approach of Bretherton et al. (2010), and accounting for both long-wave (LW) and shortwave (SW) flux, also increases to the west. When the data are binned longitudinally, the flux divergence increases by nearly the same factor as the LHF, and the average ratio $\Delta F_R/\mathrm{LHF} \approx 0.4-0.65$. However, this is biased somewhat by the flight plan, in which the near shore region is sampled both in the early morning on the outbound flights, and later in the day on the return trip when SW forcing is significant, while the far west region is sampled primarily in the early morning. When the sample is restricted to morning (before 09:00 local time), non-precipitating legs (for which the expression given by (7) is most applicable), the LHF increases from 70 W m^{-2} near shore to 135 W m^{-2} offshore, while ΔF_R increases from 71 W m^{-2} to 95 W m^{-2}, a much less significant increase than the LHF.

Based on these arguments, the left-hand side of (7) typically ranges from 1 near the coast to 0.7 at 85° W, and the typical ratio of the right hand side to the left hand side varies from 0.3 near the coast to 0.9 at 85° W. A ratio of 0.4 roughly corresponds to the observed decoupling threshold. The idealized model suggests this threshold ratio should be the larger value of 1, but does correctly predict that decoupling should be

ACPD
11, 8431–8460, 2011

much more common further offshore, and also correctly predicts that the variation of $\Delta z_M/z_i$ is the most important factor modulating this tendency. Correcting for the effect of precipitation might help bring the Bretherton and Wyant (1997) model into better quantitative agreement with the data.

The idealized model suggests that for fixed $\Delta z_M/z_i$, increased LHF might help induce decoupling. Figure 9 shows our bulk estimate of LHF vs. longitude, with decoupled legs colored in red. In contrast to Fig. 7, there is no clear separation of well-mixed from decoupled legs at any given longitude. It is thus our interpretation that although there is a correlation between LHF and decoupling, LHF does not play the dominant role in determining decoupling in VOCALS-REx. In fact, no other combination of parameters appearing in Eq. (7) is able to reliably classify a decoupled profile as well as Δz_M.

3.1 Inversion jumps

Past studies have suggested jumps of moist thermodynamic properties between the inversion base and top are an important control on stratocumulus entrainment, cloud fraction and decoupling. Randall (1980) hypothesized that if these jumps supported the production of negatively buoyant mixtures of cloudy and above-inversion air ("buoyancy reversal"), a runaway cloud-top entrainment instability would evaporate the cloud; this process would also decouple the boundary layer due to the strong associated downward entrainment flux of warm air below cloud base. While prior field observations have shown frequent examples of stratocumulus persisting despite buoyancy reversal (Kuo and Schubert, 1988), they do not rule out more stringent instability criteria that have been proposed since (e.g. MacVean and Mason, 1990). Many stratocumulus entrainment parametrizations build in some enhancement of the efficiency of entrainment with increasing buoyancy reversal (e.g. Nicholls and Turton, 1986; Lock, 2000). Recently, a set of large-eddy simulations by Lock (2009) showed a strong relation between stra-

ACPD
11, 8431–8460, 2011
VOCALS decoupling
C. R. Jones et al.

tocumulus cloud cover and a ratio of inversion humidity and temperature jumps

$$\kappa = 1 + \frac{\delta\theta_\ell}{(L/c_p)\delta q_T}, \tag{9}$$

where c_p is the specific heat capacity of dry air and δx indicates the difference between x just above the inversion and just below the inversion. κ provides a measure of the buoyancy of air parcels at the cloud top formed by mixing cloudy air with air from just above the inversion, and is thus related to the entrainment rate. Buoyancy reversal occurs for $\kappa > 0.23$ and becomes more pronounced for larger κ. The large-eddy simulations presented by Lock (2009) maintained solid stratocumulus cover for $\kappa < 0.4$, with a smooth transition for $0.4 < \kappa < 0.5$ to cloud fractions less than 20%.

We examined the relationship between inversion jumps, cloud fraction, and decoupling in the REx C-130 profile dataset. The top of the entrainment zone was identified as the minimum height above the inversion for which both the relative humidity and temperature gradients remained sufficiently small ($\left|\frac{d\mathrm{RH}}{dz}\right| < 0.3\%\,\mathrm{m}^{-1}$, $\frac{d\theta_\ell}{dz} < 0.1\,\mathrm{K\,m}^{-1}$) for a vertical range of 100 m, and the relative humidity was within 10% of the profile-minimum. This procedure works well for identifying the entrainment zone when the capping inversion is sharp, as is typical in VOCALS-REx (see, for example, Fig. 2).

Within POCs, however, the entrainment zone tends to be thicker and the inversion more diffuse, resulting in a more complex inversion structure for which this approach is insufficient to adequately identify the inversion jump. Figure 10 shows the inversion structure from a sample POC profile. The inversion top identified by the above method, shown as a solid red line, does not extend high enough to capture the full moisture and temperature jump. Thus, for POC profiles we instead determine the inversion top visually, choosing the height which best reflects the temperature and moisture in the free troposphere. The dashed red line marks the visually-identified inversion top that was used to calculate κ for this profile.

For each profile that had an adjacent subcloud leg, we calculated a lidar-derived cloud fraction averaged over the 10 minutes of the subcloud leg closest to the profile.

ACPD
11, 8431–8460, 2011

To control for the strong diurnal cycle of cloud fraction, we restricted cloud fraction measurements to profiles occurring before 10:00 local time (LT).

Portions of several RFs were devoted to investigating POCs, and the flight plan of these flights required a more sophisticated approach to link POC profile and subcloud leg for determining the cloud fraction, to ensure that both the profile and subcloud leg were within the POC region. The flight plan was such that there was typically only one morning subcloud leg that extended into the POC, with several POC profiles. For each POC subcloud leg, we identified the region that was within the POC using GOES-10 thermal infrared satellite images from the time of the subcloud leg, and then found the nearest spatially collocated POC profile. Before 10:00 LT, there are only 3 POC profiles associated with a subcloud leg, occurring in RF07-RF09. Missing from these is RF06, a POC flight featured in Wood et al. (2010). We were unable to reliably determine the inversion jumps from RF06 because the fast-response Lyman-alpha hygrometer was inoperative on this flight.

Figure 11 shows scatter plots between κ and cloud fraction, Δq, and Δz_b in the C-130 profile datasets. The middle and right panels suggest that decoupling is not correlated to κ. Among the pre-10:00 LT profiles with which we can associate a cloud fraction, it is 100% for most cases with $\kappa < 0.5$, and in almost all cases with $\kappa < 0.25$. However, once κ exceeds approximately 0.3, there are a number of cases with partial cloud cover. These observations are qualitatively consistent with the large-eddy simulation results presented in Lock (2009), though the observed cloud fraction tends to be somewhat larger at a given κ than the range suggested by the simulations, which is shown by the pair of dashed curves.

Data points from profiles within POCs are indicated in red in Fig. 11). From the middle panel we can gather that the POC regions were all decoupled with $\kappa > 0.28$. The three POC profiles with a corresponding cloud fraction are plotted in the left panel. These fall on the low edge of the non-POC profiles, consistent with cloud-aerosol-precipitation feedbacks reducing cloud fraction in POCs compared to surrounding stratocumulus with similar inversion jumps.

ACPD
11, 8431–8460, 2011

VOCALS decoupling

C. R. Jones et al.

4 Conclusions

We used profiles and subcloud legs from VOCALS-REx to classify each leg as well-mixed or decoupled. We find the well-mixed cloud thickness Δz_M to be the best predictor for decoupling observed in VOCALS-REx. This is shown most strikingly by the sharp distinction between the range of values of Δz_M for coupled and decoupled subcloud legs in Fig. 7, in which legs are typically decoupled when $\Delta z_M > 500$ m, and well-mixed otherwise.

This empirical threshold for decoupling occurs at approximately the same cloud thickness where precipitation can be expected to become significant. Similarly, we also note that LHF, another factor in driving boundary layer decoupling, increases to the west along with the prevalence of decoupling. Each of these mechanisms likely plays an important role in decoupling in VOCALS-REx. However, no other parameter is able to predict decoupling as consistently as Δz_M.

In general, the inversion jump parameter κ was found not to be a good predictor of decoupling. Coupled and decoupled profiles are well-distributed across the range of κ values. The only possible exception to this is for very large values of κ. Though it represents a small sample of points from which no definitive conclusion can be drawn, all 8 profiles with $\kappa > 0.5$ were found to be decoupled. Most of these profiles were within POCs.

While κ is not a good predictor for decoupling, we do find that a low cloud fraction is nearly always associated with a high κ. Decoupling in itself is not a good predictor for low cloud fraction, and many subcloud legs classified as decoupled were nearly 100% cloud covered.

Acknowledgements. The authors gratefully acknowledge support from NSF grant ATM 0745702 (CB) and ATM-0745986 (DL) and a Boeing Endowed Professorship in Applied Mathematics awarded to CB. The RAF C-130 measurements were obtained from the VOCALS data archive of NCAR/EOL, which is sponsored by the NSF. Chris Terai helped prepare the C-130 profile dataset. Rob Wood provided much helpful advice.

ACPD
11, 8431–8460, 2011

References

Bretherton, C. S. and Wyant, M. C.: Moisture transport, lower-tropospheric stability, and decoupling of cloud-topped boundary layers, J. Atmos. Sci., 54, 148–167, 1997. 8433, 8434, 8440, 8442, 8443, 8444

Bretherton, C. S., Uttal, T., Fairall, C. W., Yuter, S., Weller, R., Baumgardner, D., Comstock, K., and Wood, R.: The EPIC 2001 stratocumulus study, B. Am. Meteorol. Soc., 85, 967–977, 2004.

Bretherton, C. S., Wood, R., George, R. C., Leon, D., Allen, G., Zheng, X.: Southeast Pacific stratocumulus clouds, precipitation and boundary layer structure sampled along 20 S during VOCALS-REx, Atmos. Chem. Phys., 10, 10639–10654, doi:10.5194/acp-10-10639-2010, 2010. 8434, 8435, 8436, 8437, 8443

Caldwell, P., Bretherton, C. S., and Wood, R.: Mixed-layer budget analysis of the diurnal cycle of entrainment in Southeast Pacific stratocumulus, J. Atmos. Sci., 62, 3775–3791, 2005. 8442

Kuo, H. and Schubert, W.: Stability of cloud-topped boundary-layers, Q. J. Roy. Meteorol. Soc., 114, 887–916, 1988. 8444

Lilly, D.: Models of cloud-topped mixed layers under a strong inversion, Q. J. Roy. Meteorol. Soc., 94, 292–309, 1968. 8433

Lock, A., Brown, A.,Bush, M., Martin, G., and Smith, R.: A new boundary layer mixing scheme. Part I: Scheme description and single-column model tests Mon. Weather Rev., 128, 3187–3199, 2000. 8444

Lock, A. P.: Factors influencing cloud area at the capping inversion for shallow cumulus clouds, Q. J. Roy. Meteorol. Soc., 135, 941–952, 2009. 8444, 8445, 8446, 8460

MacVean, M. K. and Mason, P. J.: Cloud-top entrainment instability through small-scale mixing and its parameterization in numerical-models, J. Atmos. Sci., 47, 1012–1030, 1990. 8444

Nicholls, S.: The dynamics of stratocumulus–aircraft observations and comparisons with a mixed layer model, Q. J. Roy. Meteorol. Soc., 110, 783–820, 1984. 8433

Nicholls, S. and Turton, J.: An observational study of the structure of stratiform cloud sheets .2. entrainment, Q. J. Roy. Meteorol. Soc., 112, 461–480, 1986. 8444

Randall, D.: Conditional instability of the 1st kind upside-down, J. Atmos. Sci., 37, 125–130, 1980. 8444

Turton, J. D. and Nicholls, S.: A study of the diurnal-variation of stratocumulus using a multiple mixed layer model, Q. J. Roy. Meteorol. Soc., 113, 969–1009, 1987. 8433

Wood, R., Bretherton, C.S., Leon,D., Clarke, A. D., Zuidema, P., Allen, G., and Coe, H.: An aircraft case study of the spatial transition from closed to open mesoscale cellular convection over the Southeast Pacific, Atmos. Chem. Phys. Discuss., 10, 17911–17980, doi:10.5194/acpd-10-17911-2010, 2010. 8446

Wood, R., Mechoso, C. R., Bretherton, C. S., Weller, R. A., Huebert, B., Straneo, F., Albrecht, B. A., Coe, H., Allen, G., Vaughan, G., Daum, P., Fairall, C., Chand, D., Gallardo Klenner, L., Garreaud, R., Grados, C., Covert, D. S., Bates, T. S., Krejci, R., Russell, L. M., de Szoeke, S., Brewer, A., Yuter, S. E., Springston, S. R., Chaigneau, A., Toniazzo, T., Minnis, P., Palikonda, R., Abel, S. J., Brown, W. O. J., Williams, S., Fochesatto, J., Brioude, J., and Bower, K. N.: The VAMOS Ocean-Cloud-Atmosphere-Land Study Regional Experiment (VOCALS-REx): goals, platforms, and field operations, Atmos. Chem. Phys., 11, 627–654, doi:10.5194/acp-11-627-2011, 2011. 8434, 8436

ACPD
11, 8431–8460, 2011

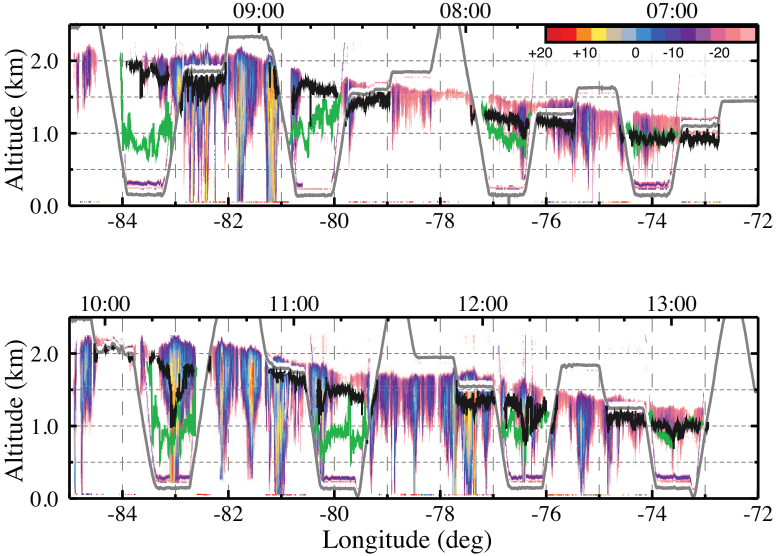

Fig. 1. (top) Time-height sections of RF04 WCR 94 GHz cloud radar reflectivity (dBZ scale shown in the upper right of the top panel). Top panel: outbound flight, bottom panel: return flight. Lidar cloud base during subcloud legs is shown in black, LCL from in-situ measurements is shown in green, and flight path is shown in grey.

ACPD
11, 8431–8460, 2011

VOCALS decoupling

C. R. Jones et al.

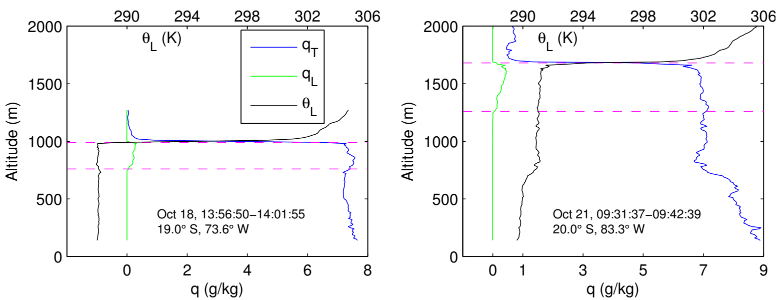

Fig. 2. Typical well-mixed (left) and decoupled (right) profiles of moist-conserved variables. The dashed magenta lines demarcate the cloud layer.

ACPD
11, 8431–8460, 2011

VOCALS decoupling

C. R. Jones et al.

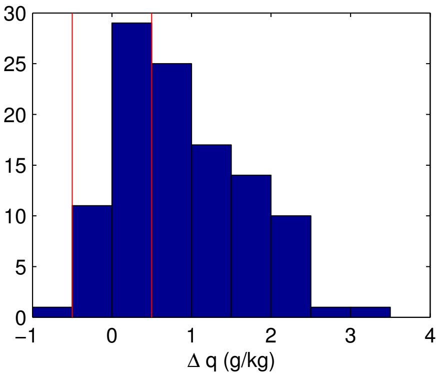

Fig. 3. Histogram of Δq with the "well-mixed" classification $|\Delta q| < 0.5$ g/kg indicated by the red vertical lines.

ACPD
11, 8431–8460, 2011

VOCALS decoupling

C. R. Jones et al.

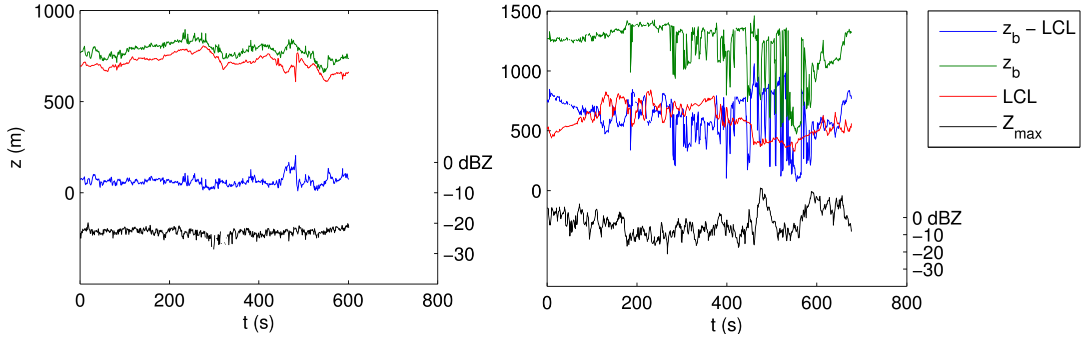

Fig. 4. Cloudbase and LCL of the subcloud legs adjacent to the profiles shown in Fig. 2, showing an example of the mesoscale structure associated with a well-mixed (left) and decoupled (right) boundary layer.

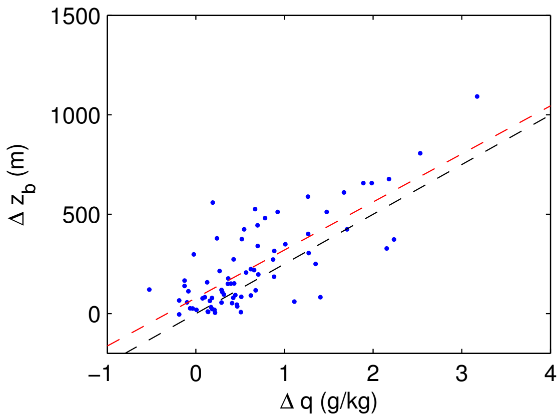

Fig. 5. The profile decoupling index Δq and the decoupling measurement from the adjacent subcloud leg Δz_b provide a consistent metric for determining decoupling. The dashed black line has slope 125 m per 0.5 (g/kg), and the dashed red line is the linear least squares fit.

ACPD
11, 8431–8460, 2011

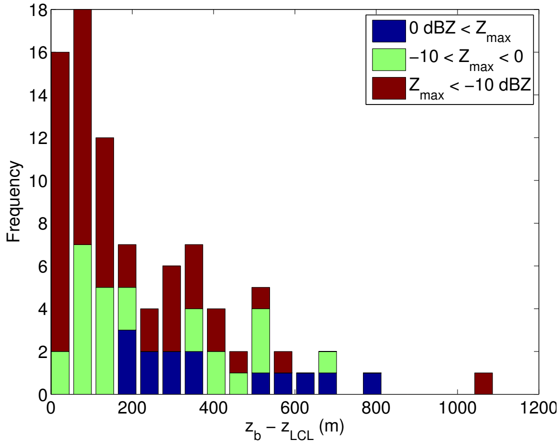

Fig. 6. Mean cloud base – LCL (Δz_b) for each subcloud leg. Each bin is also separated based on drizzle.

ACPD
11, 8431–8460, 2011

Title Page
Abstract Introduction
Conclusions References
Tables Figures
◀ ▶
Back Close
Full Screen / Esc
Printer-friendly Version
Interactive Discussion

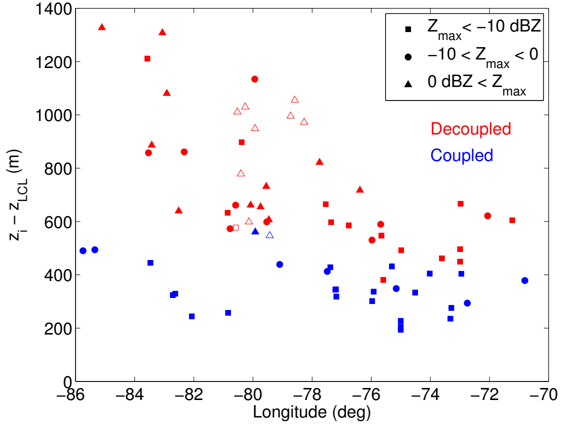

Fig. 7. Decoupling, well-mixed cloud thickness Δz_M, and drizzle by longitude for each subcloud leg. Blue (red) markers indicate well-mixed (decoupled) legs. Moderately drizzling legs are indicated by triangles, lightly drizzling legs by circles, and nondrizzling legs by squares. POC legs are indicated by hollow markers.

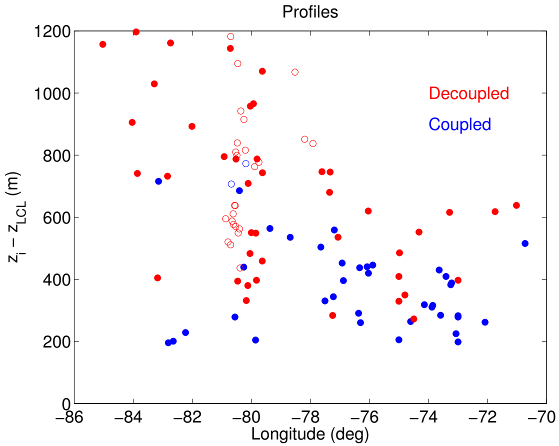

Fig. 8. Decoupling and well-mixed cloud thickness Δz_M by longitude for each profile. Blue (red) markers indicate well-mixed (decoupled) profiles. POC profiles are indicated by the hollow markers.

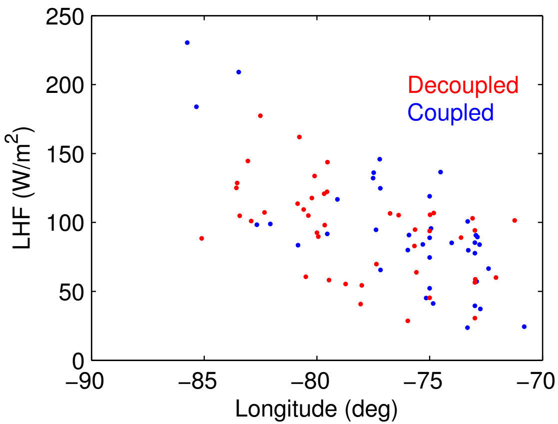

Fig. 9. Latent heat flux by longitude for each subcloud leg. Blue (red) markers indicate well-mixed (decoupled) subcloud legs.

ACPD
11, 8431–8460, 2011

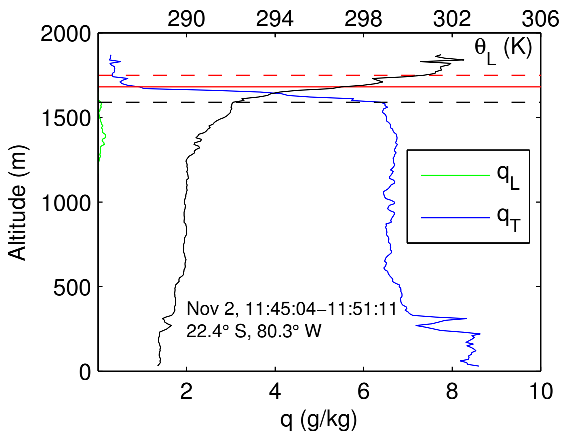

Fig. 10. Liquid water mixing ratio (green), total water mixing ratio (blue), and liquid potential temperature (black) profiles illustrating the inversion structure observed in a typical POC profile. The dashed black line marks the inversion base. The inversion top deduced using the criteria described in Sect. 3.1 is indicated by the solid red horizontal line, whereas the visually determined inversion top used to calculate κ is indicated by the dashed red line.

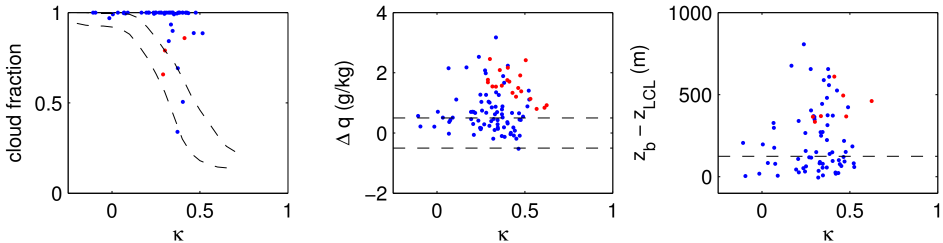

Fig. 11. Cloud fraction (left), profile decoupling index (middle), and subcloud decoupling index (right) as a function of the inversion jump parameter κ. Data from POC flights are shown in red. Dashed lines in the middle and right panel indicate the decoupling threshold. Only profiles and legs before 10:00 local time are included in the left panel to reduce the influence of diurnal forcing on the cloud fraction. The dashed curves in the left panel correspond to the range of LES results presented in Lock (2009).